Journal of Statistical Physics, Vol. 128, Nos. 1/2, July 2007 (© 2007)
DOI: 10.1007/s10955-007-9298-9

A New Mechanism for Collective Migration in *Myxococcus xanthus*

J. Starruß,[1] Th. Bley,[2] L. Søgaard-Andersen[3] and A. Deutsch[1]

Received March 23, 2006; accepted January 31, 2007
Published Online March 23, 2007

Myxobacteria exhibit a complex life cycle characterized by a sequence of cell patterns that culminate in the formation of three-dimensional fruiting bodies. This paper provides indications that the specific cell shape of myxobacteria might play an important role in the different morphogenetic processes during the life cycle. We introduce a new mechanism for collective migration that can explain the formation of aligned cell clusters in myxobacteria. This mechanism does not depend on cell cooperation, and in particular it does not depend on diffusive signals guiding cell motion.

A *Cellular Potts Model* (CPM) that captures the rod cell shape, cell stiffness and active motion of myxobacteria is presented. By means of numerical simulations of model cell populations where cells interact via volume exclusion, we provide evidence of a purely mechanical mechanism for collective migration, which is controlled by the cells' length-to-width aspect ratio.

KEY WORDS: Cellular Potts Model, cellular automata, collective migration, rod-shaped cells, myxobacteria.

1. INTRODUCTION

Collective migration is a prominent example of complex behaviour in biological systems. Single entities organize into clusters, align their orientations and directions of movement and start to act as a kind of community. In populations of the rod-shaped bacterium *Myxococcus xanthus* collective migration

[1] Center for Information Services and High Performance Computing, Technische Universität Dresden, Dresden, Germany; e-mail: joern.starruss@tu-dresden.de.
[2] Instiute of Food Technologies and Bioprocess Engineering, Technische Universität Dresden, Dresden, Germany.
[3] Max Planck Institute for Terrestrial Microbiology, Marburg, Germany.

can be easily observed and thoroughly studied under laboratory conditions. We introduce a mechanism for collective migration and the formation of aligned cell clusters, which is purely mechanical and might explain the respective phenomena in myxobacteria.

Myxobacteria are characterized by a complex life cycle, consisting of a growth part and a developmental part. In the growth part thousands of cells move and proliferate to form a spreading colony. The colony primarily expands due to movement of cells, thus, leading to the formation of a spreading zone at the edge of a colony.[10,12] Upon depletion of nutrients the developmental part of the life cycle is initiated. The population passes through a well defined sequence of developmental stages – rippling, streaming, aggregation – and finally forms three-dimensional multicellular fruiting bodies. This complex morphogenetic process starts from an almost unstructured population and might offer valuable clues to a better understanding of multicellular development.

Collective migration can be observed in several stages of the life cycle. In particular, collective migration is visible through the formation of aligned cell clusters, which move into the same direction. The size of the migrating cell clusters, i.e. the number of constituent cells, differs greatly during the life cycle. The largest aligned cell clusters arise in the streaming phase and lead to cell aggregation. In this particular phase, aligned cell clusters may be viewed as a prepattern for subsequent patterning processes. In a spreading colony, smaller aligned cell clusters form in the spreading zone: Often cells are observed to leave the compact part of the colony and enter the spreading zone in a flare-like fashion, circle around and then rejoin the compact part.[10,11] Also within the compact part of a colony cells are often organized into small aligned clusters. These observations lead to the hypothesis that the phenomenon of collective migration is not linked to a certain phase of the life cycle, but rather a general feature, whose intensity varies during the life cycle.

Essential for myxobacterial pattern formation is coordinated motion.[10,18] Myxobacteria move by gliding on solid surfaces and harbour two different motility systems: The A-motility system for individual cell motion and the S-motility system for "social" cell motion. The A-motility engine is hypothesized to be based on slime extrusion from the lagging cell pole, however, the particular mechanism remains unknown. The S-motility engine is based on the retraction of type IV pili.[18] Pili are extended from the leading cell pole, attach to neighbouring cells and force is generated upon retraction. Thus, the S-motility system is cooperative and requires cells to be in close proximity. Collective motion is not specifically linked to either the A- or the S-motility system – aligned cell clusters can appear in cell populations with only one active motility system, but S-motility requires high cell densities and soft agar surfaces to become active.[17,19]

In *M. xanthus* cell motion is characterized by regular reversals of the direction of movement due to the simultaneous change in polarity of the two motility

engines. The frequency of cell reversals is a parameter that changes drastically during the life cycle and thereby affects the cell patterns formed by the population. In the growth part cells on the average reverse every 10 min and small aligned cell clusters are observed.[10] Early in the developmental part reversals become more frequent and cells synchronize their reversal, which leads to the formation of rippling patterns.[2,7,9,24] In the subsequent streaming phase collectively migrating clusters arise again and grow to large sizes. This phase is characterized by a monotonously decreasing reversal frequency and by an increase of cell speed, up to a point where the cell movement becomes nearly unidirectional.[9,10] This cell behaviour coincides with the emergence of the largest aligned cell clusters in *M. xanthus,* leading to the hypothesis that unidirectional motion, i.e. persistence, is beneficial for the myxobacterial mechanism of collective migration.

Comparable collective migration behaviour, which also leads to aggregation and fruiting body formation, is well known in the slime mould *Dictyostelium discoideum*.[15] Indeed *D. discoideum* and *M. xanthus* share significant similarities in the cell patterns leading to fruiting body formation. However, no signal corresponding to the diffusive cAMP signal, which guides cell movement in *D. discoideum*, has been identified in myxobacteria. Moreover, various models for myxobacterial rippling indicate that local cell interaction via the membrane-bound C-signal, which regulates the reversal frequency, can account for the formation of macroscopic cell patterns in *M. xanthus*.[2,7]

Collective migration, also referred to as 'swarming,' in self-propelled particles has been extensively studied under the assumption of local cooperation between the individuals, e.g. by considering that individuals choose the average orientation of their neighbours.[3,4,14,23] Lately a cooperative mechanism that mediates local cell alignment via optimizing C-signal transmission between cells has been suggested by Alber *et al.*[1] to account for pattern formation in myxobacteria.

Here we present a new mechanism for collective migration in myxobacteria that does not incorporate any cooperative mechanism. We propose that aligned cell clusters and collective migration in myxobaceria arise due to the following inherent properties of each individual cell: the specific length-to-width aspect ratio, cell stiffness and active cell motion. Although cooperative mechanisms, esp. adhesion and signaling, have an impact on the myxobacterial pattern formation, we propose they are not essential for clustering. We suggest that collision of rod-shaped cells induces local cell alignment and accounts for the formation of macroscopic aligned cell clusters. For the following model investigation we furthermore consider nonreversing cells, which move unidirectionally and are known to form the largest cell clusters.[9,10]

A suitable method for testing this hypothesis is to develop a mathematical model, incorporating the single cell properties mentioned above. So far mathematical models applied to myxobacterial pattern formation paid almost no attention

to the anisotropy of the cell shape (e.g. Refs. 2, 8). In the models, mechanical cell interaction is typically approximated by local averaging of the cell orientations. One exception is the stochastic model by Stevens,[21] in which a biological cell is represented by a set of connected discrete lattice nodes and cells interact via volume exclusion. Here, we extend the idea of a discrete stochastic model and increase the resolution of the cell shape approximation and the freedom in movement (including cell deformation). The *Cellular Potts Model* (CPM), which has recently been used to model elongated epithelial cells,[13] has been adapted to represent myxobacterial cells.

Rod-shaped model cells are depicted in our model using the concept of a "segmented cell," where a connected row of CPM cells approximates the elongated shape of myxobacteria. The stiffness of the model cell is defined as optimality criterion for the positioning of the cell segments by using energetic constraints.

We will introduce the model in Sec. 2 and characterize the behaviour of a single model cell in the first part of the results (Sec. 3.1). Simulations of macroscopic collective migration in model cell populations are presented in Sec. 3.2 and we give a broad discussion in Sec. 4.

2. MODEL DEFINITION

Our model builds on the *Cellular Potts Model* (CPM),[6] a lattice-based model, that represents a biological cell as a connected set of lattice nodes and lets the cells interact along their boundary with their neighbours (cells or medium). This interaction is modelled via an interaction energy in the global Hamiltonian $\mathcal{H}$, the system's free energy. Further constraints at the individual cell level, e.g. a limited compressibility, can be taken into account via additional terms in the Hamiltonian.

We developed a model for rod-shaped cells using the concept of a segmented cell. Along its long axis, each model cell μ is subdivided into cell segments ν, that are formed by original *Cellular Potts model* cells. We do not assume any biological interpretation of this segmentation.

We define a two-component state σ of a lattice node $\mathbf{i} \in \mathbb{L} \subset \mathbb{Z}^2$.

$$\sigma(\mathbf{i}) = (\mu, \nu) \in \mathbb{S} = \{(0,0),\ (k,l),\ k \in \{1,\ldots,c\},\ l \in \{1,\ldots,s\}\}, \qquad (1)$$

where c is the number of cells and s the number of segments per cell. A lattice node $\mathbf{i}$ with $\sigma(\mathbf{i}) = (\mu, \nu)$ is now occupied by the νth segment of cell μ or by medium if $\sigma(\mathbf{i}) = \sigma_0 = (0,0)$. We assign an order to the cell segments by denoting the first cell segment ($\nu = 1$) "head" and the last cell segment ($\nu = s$) "tail."

Fig. 1. Scheme of a segmented model cell on a hexagonal lattice. Head and tail segments are indicated by darker grey values. The figure shows the curvature radius R_{curve} and the segment distance D. ($\mathbf{S}_{\mu,\nu_n}$ specifies the centre of mass of the segment ν_n of cell μ).

2.1. Hamiltonian

In addition to the boundary-dependent energy and the volume constraint already included in the Hamiltonian of the original CPM we use energetic constraints for the cell deformation: a length and a curvature energy. For the purpose of simplification we initially define $\mathbf{S}_{\mu,\nu}$ to be the centre of mass of the νth segment of cell μ. The curvature energy in our model depends on the radius of the cell's curvature, comparable to the bending energy of solid bodies. Under the assumption of low curvature, each three consecutive cell segments in our model allow the following approximation of the radius (Fig. 1)

$$R_{\text{curve}}(\mathbf{S}_{\mu,\nu}, \mathbf{S}_{\mu,\nu+1}, \mathbf{S}_{\mu,\nu+2}) = \frac{|\mathbf{S}_{\mu,\nu+2} - \mathbf{S}_{\mu,\nu}|}{2\,\sin(\measuredangle(\mathbf{S}_{\mu,\nu}, \mathbf{S}_{\mu,\nu+1}, \mathbf{S}_{\mu,\nu+2}))}. \tag{2}$$

Thus, we can define the curvature energy of cell μ as a segment-wise sum of $E_{\text{curve}}(\nu) \sim 1/R^2$ with the sensitivity parameter ξ,

$$E_{\text{curve}}(\mu) = \xi \sum_{\nu=1}^{s-2} (1/R_{\text{curve}}(\mathbf{S}_{\mu,\nu}, \mathbf{S}_{\mu,\nu+1}, \mathbf{S}_{\mu,\nu+2}))^2. \tag{3}$$

A second energy E_{length} (length energy) reflects the process of stretching and shortening of a cell. Equation (4) is based on the comparison of the distance of neighbouring cell segments and an optimal distance D and is defined as the following squared sum with sensitivity parameter ζ

$$E_{\text{length}}(\mu) = \zeta \sum_{\nu=1}^{s-1} (|\mathbf{S}_{\mu,\nu} - \mathbf{S}_{\mu,\nu+1}| - D)^2. \tag{4}$$

The extended Hamiltonian of the model is defined as:

$$\begin{aligned}\mathcal{H} = & \sum_{\langle \mathbf{i},\mathbf{j}\rangle \text{neighbours}} \tfrac{1}{2} J_{\sigma(\mathbf{i}),\sigma(\mathbf{j})} \\ & + \lambda \sum_{\mu=1}^{c} \sum_{\nu=1}^{s} (a_{\mu,\nu} - A)^2 \\ & + \zeta \sum_{\mu=1}^{c} \sum_{\nu=1}^{s-1} (|\mathbf{S}_{\mu,\nu} - \mathbf{S}_{\mu,\nu+1}| - D)^2 \\ & + \xi \sum_{\mu=1}^{c} \sum_{\nu=1}^{s-2} (1/R_{\text{curve}}(\mathbf{S}_{\mu,\nu},\ \mathbf{S}_{\mu,\nu+1},\ \mathbf{S}_{\mu,\nu+2}))^2 \end{aligned} \tag{5}$$

The interaction energy J_{σ_1,σ_2} used in (5) depends on the type of interacting states σ. For cell-cell interaction we define an energy J_{CC} and for cell-medium J_{CM} (6). In order to keep the segments of one cell attached but unmixed, we define a reduced interaction energy J_{SS} between nodes of neighbouring segments.

$$J_{\sigma_1,\sigma_2} = J_{(\mu_1,\nu_1),(\mu_2,\nu_2)} = \begin{cases} 0 & \text{if } \sigma_1 = \sigma_2, \\ J_{CM} & \text{if either } \sigma_1 = (0,0) \text{ or } \sigma_2 = (0,0), \\ J_{SS} & \text{if } \mu_1 = \mu_2 \neq 0 \text{ and } |\nu_1 - \nu_2| = 1, \\ J_{CC} & \text{else.} \end{cases} \tag{6}$$

The second term in (5), the volume constraint, models a limited compressibility of a cell segment by comparing the number of nodes occupied by a cell segment $a_{\mu,\nu}$ to an optimal value A.

2.2. Simulation and Active Motion

The algorithm for simulating a time series remains as described for the original CPM.[6] Starting from an initial lattice configuration updates ($\sigma(\mathbf{i}) \to \sigma(\mathbf{j})$) are performed as follows: a node $\mathbf{i}$ is selected at random and its state is converted to the state of one of its nearest neighbours $\mathbf{j}$ with a success probability p depending on the change in free energy due to this "copy operation" (Metropolis-Kinetics (7))

$$p(\Delta\mathcal{H}') = \begin{cases} 1 & \text{if } \Delta\mathcal{H}' < 0 \\ e^{\frac{\Delta\mathcal{H}'}{kT}} & \text{if } \Delta\mathcal{H}' \geq 0. \end{cases} \tag{7}$$

The total change in energy

$$\Delta\mathcal{H}' = \Delta\mathcal{H} + \Delta D \tag{8}$$

sums the change in free energy and the propulsive energy ΔD, which is described next.

The active motion of a single cell was modelled by an energetic advance of updates shifting the cell into its moving direction, defined by the propulsion energy ΔD. The moving direction of an actively moving cell basically depends on its local orientation, i.e. on the positioning of the cell segments. Thus, a segment's moving direction is directed from its succeeding to its preceding cell segment, while the moving direction of an edge segment ($\nu = 1$ or $\nu = s$) is equal to the moving direction of its neighbouring segment (9). Since the medium does not actively move, we set its moving direction $\theta(\sigma_0) = \mathbf{0}$.

$$\theta_\sigma = \theta_{\mu,\nu} = \begin{cases} \mathbf{0} & \text{if } \mu = \nu = 0, \\ \theta_{\mu,\nu+1} & \text{if } \nu = 1, \\ \theta_{\mu,\nu-1} & \text{if } \nu = s, \\ ||\mathbf{S}_{\mu,\nu-1} - \mathbf{S}_{\mu,\nu+1}|| & \text{else.} \end{cases} \tag{9}$$

We consider a single update $\sigma(\mathbf{i}) \to \sigma(\mathbf{j})$ to shift the segments $\sigma(\mathbf{i})$ and $\sigma(\mathbf{j})$ into the update direction $\mathbf{d} = \mathbf{i} - \mathbf{j}$. Thus, a propulsion energy ΔD can be obtained by comparing the update direction with the moving directions of the involved cell segments according to Eq. (10) via a scalar product. The parameter ω indicates the strength of the energetic advance, i.e. propulsion. In the case that one of the involved nodes belongs to the medium one of the terms in (10) will vanish due to $\theta(\sigma_0) = \mathbf{0}$.

$$\Delta D(\sigma(\mathbf{i}) \to \sigma(\mathbf{j})) = -\omega\big(\mathbf{d} \circ \theta_{\sigma(\mathbf{i})} + \mathbf{d} \circ \theta_{\sigma(\mathbf{j})}\big) \tag{10}$$

2.3. Numerical Simulation

Numerical simulations were executed on a hexagonal lattice $\mathbb{L} \subset \mathbb{Z}^2$ with periodical boundary conditions.[4] Second-nearest neighbours were used for the calculation of node interaction energy J_{σ_1,σ_2} in (5). The specific choice of the lattice geometry and neighbourhood allows a sufficently high number of possible moving directions.

Parameter estimation was performed in two steps: first for internal parameters, i.e. parameters that do not rely on the behaviour of the biological cell, and subsequently for biological parameters. Internal parameters were chosen to assure:

- spatial integrity of a cell (volume exclusion),
- spatial separation of segments within a cell,
- motility in the discrete space.

[4] The centres of mass of the segments within a cell were calculated in a non-periodic space after projection $\mathbb{L} \to \mathbb{Z}^2$.

Table I. Parameter set 'xanthus'—Model Parameters Estimated for *Myxococcus xanthus*. Energetic Values are Given in the Arbitrary Unit $\mathfrak{E}$.

Target area of a segment	$A = 12$
Target distance of neighboring segments within a cell	$D = \sqrt{A}$
Cell – medium interaction energy	$J_{CM} = 1\,\mathfrak{E}$
Cell – cell interaction energy	$J_{CC} = 3\,\mathfrak{E}$
Interaction energy between neighboring segments within a cell	$J_{SS} = 0.3\,\mathfrak{E}$
Boltzmann constant × temperature	$kT = 0.8\,\mathfrak{E}$
Number of segments per cell	$s = 8$
Strength of volume constraint	$\lambda = 0.7\,\mathfrak{E}$
Strength of propulsion	$\omega = 0.5\,\mathfrak{E}$
Sensitivity of curvature constraint	$\xi = 300\,\mathfrak{E}$
Sensitivity of length constraint	$\zeta = 35\,\mathfrak{E}$

In addition a short-range repulsion was introduced between neighbouring cells by setting $J_{CC} = 3J_{CM}$.[5] This mimics a thin film of medium between cells. The temperature parameter in our model allows to incorporate stochastic effects. The resulting parameter set 'xanthus,' shown in Table I, also lists the biological parameters. The simulations of cell populations in the results section were started from random initial configurations, where position and orientation of each cell were chosen at random.

3. RESULTS

3.1. Validation of Single Cell Concept

The *Cellular Potts Model* (CPM) is a lattice-based model that, in contrast to cellular automata,[6] represents biological cells as a connected set of lattice nodes. The dynamics of the system are defined by the Metropolis kinetics and follow the energy gradients of the system's Hamiltonian in a stochastic manner. In this section we show our model, which is derived from the CPM, to mimic single rod-shaped *M. xanthus* cells in terms of stiffness and active motion.

The stiffness of the model cell has been defined by energetic constraints penalizing cell deformation. An experimental manifestation of cell stiffness is the relaxation of an artificially bended cell. Considering high damping in the cell environment, e.g. on slime covered agar surfaces, we can neglect inertia. Thus, we expect an exponential decrease in bending energy under experimental

[5] The effective energetic disadvantage is 50% only, since energetically neutral interaction is obtained for $J_{CC} = 2J_{CM}$.

[6] Cellular automata (e.g. Ref. 4) represent individuals as point-like particles.

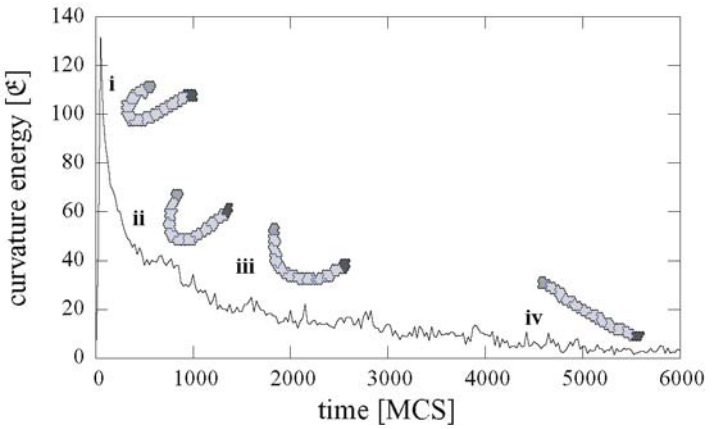

Fig. 2. The curvature energy of an artificially deformed cell decreases exponentially with time. Snapshots **i**–**iv** show the temporal development of such a simulated cell. Finally the cell becomes almost unbended and only a very low curvature energy remains (parameter set 'xanthus').

conditions.[7] We mimicked this experiment in a simulation. Figure 2i shows an initially bended cell that unbends during simulation (Figs. 2ii–iv). The Metropolis kinetics favours updates of the lattice configuration that reduce the curvature energy (E_{curve}) and thereby the curvature of the model cell. As expected we observe an almost exponential decay in curvature energy (Fig. 2).

Low values of the model temperature T result in incomplete relaxation. This indicates that the stochastic part in the simulation dynamics (visible as noise in the energy decay in Fig. 2) is necessary to overcome unfavourable intermediate configurations.

The ratio of stiffness and propulsion essentially characterizes the mechanical behaviour of a myxobacterial cell. Spormann and Kaiser[20] have observed a phenomenon which immensely depends on this cell parameter (Fig. 3). A cell whose head is fortuitously fixed in the agar performs a snake-like motion. The stiffness of the cell determines the intensity of bending due to the active motion. We simulated this experiment with a preset $\omega = 0.5\,\text{Ɛ}$ and found an analogue motion sequence for $\xi \approx 300\,\text{Ɛ}$ (Fig. 3).

The motility of the model cell has been established through an energetic advance of updates shifting a cell into its moving direction (a time series of a moving single cell is shown in Fig. 4). This means that our model cell corresponds

[7] Close to equilibrium we can assume the bending angle θ of a flexible rod to follow $I\ddot{\theta} = -\zeta\dot{\theta} - \frac{\partial U}{\partial \theta}$ (I-inertia, U-bending energy, ζ-friction coefficient). Assuming $I = 0$ and $U = k\theta^2$ (k-spring constant) results in $\dot{\theta} = -\frac{2k}{\zeta}\theta$. Thus, $\theta(t) = e^{-kt/\zeta}$.

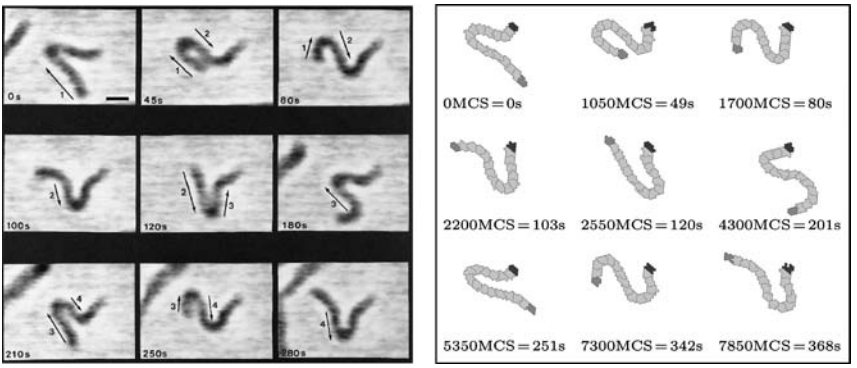

Fig. 3. Estimation of cell stiffness by simulation of a single cell experiment. The image sequence on the left shows a cell that is fortuitously fixed with its "head" in the agar.[20] A certain ratio of cell stiffness and propelling force results in the observed snakelike motion. In the initial phase the cell deformation as well as the time scale in model simulations with estimated parameters agree with the experimental results (right image sequence). Due to a slightly different path of motion the time scales diverge in the second phase.

to a non-reversing myxobacterial cell, which moves by *A*-motility rather than by *S*-motility.

We characterize the motility of a model cell by its velocity and the stability of its moving direction. Figure 5(a) shows the single cell velocity versus the length-to-width aspect ratio κ of the cell. The aspect ratio has a minimal impact on the velocity, especially in the range of myxobacterial aspect ratios ($\kappa > 4$), which agrees with the experimental results from *M. xanthus* mutants with a wide range of cell lengths.[22] However, cells with lower κ experience weaker spatial constraints for their moving direction (Fig. 5(b), for details see below) and therefore reach a slightly higher average velocity. We found the effective speed in this model system to be proportional to the driving energy gradient in a limited range (data not shown). This is due to the absence of inertia in the model, a general property of the Metropolis kinetics. From a physical point of view it is reasonable to ignore

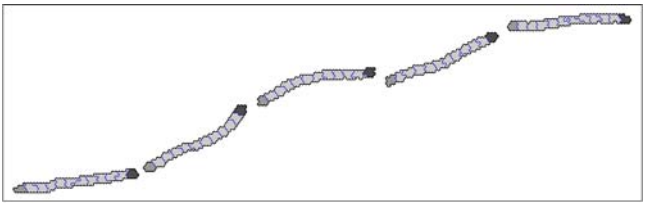

Fig. 4. Motion of a single cell for approx. 10000 MCS. Shown is the temporal sequence of a single cell (parameter set 'xanthus').

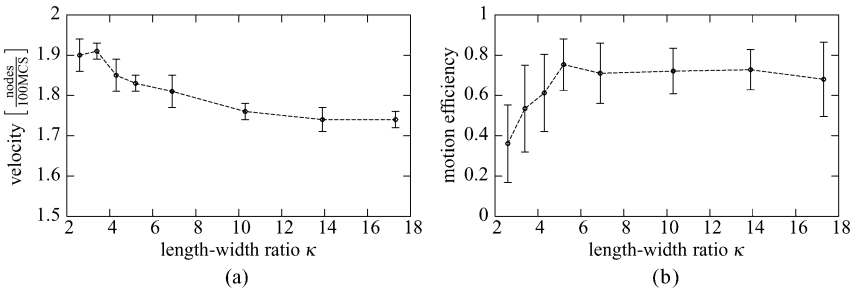

Fig. 5. The velocity of a single cell is almost independent of the length-width ratio (a). Subfig. (b) shows the motion efficiency (ratio of the net distance and a given total path length) versus the length-width ratio κ. Up to $\kappa = 5$ additional cell segments stabilize the orientation of the cell resulting in higher net gliding distances (parameter set 'xanthus,' κ was adjusted through the number of segments s per cell; mean of 15 runs; error bars indicate the standard deviation).

inertia because of the high friction between the cell and the agar surface. For the simulations, however, we kept the whole population at a constant average velocity ($\omega = \text{const.}$).

Cell motion in both situations, experiment and simulation, is not straight ahead (Fig. 4). It is affected by random changes in the moving direction. In the model the stochastic changes are mainly introduced by the stochastic update algorithm. We analysed the model cell's persistence into the moving direction by means of the motion efficiency, i.e. the ratio of net distance covered[8] and the total path length. The results shown in Fig. 5(b) indicate changes in the moving direction for all length-to-width aspect ratios. But setting the anisotropy of the cells below $\kappa = 5$ results in lower moving efficiency. The orientation stability is reduced due to the fewer number of cell segments. The simulations also elucidate, that model cells are slightly influenced by the anisotropy of the model space, leading to a preferred motion along symmetry axes of the hexagonal lattice. However, this effect was not detectable in the simulations of interacting cell populations.

Volume exclusion is an intrinsic feature of the lattice-based model. In addition, the model has to avoid interpenetration of cells, i.e. the cell segments have to be kept connected. Accordingly, the ranges for the propulsion strength ω and the temperature T are limited. The cell shape approximation that results from the estimated parameter set 'xanthus' is shown in the snapshots of Fig. 4. The cell segments always remain connected (Snapshots are presented without any steps of 'annealing'). The principle of volume exclusion is also preserved under conditions of cell collision as shown below (Sec. 3.2).

[8] Net distance: absolute distance between start and endpoint of motion.

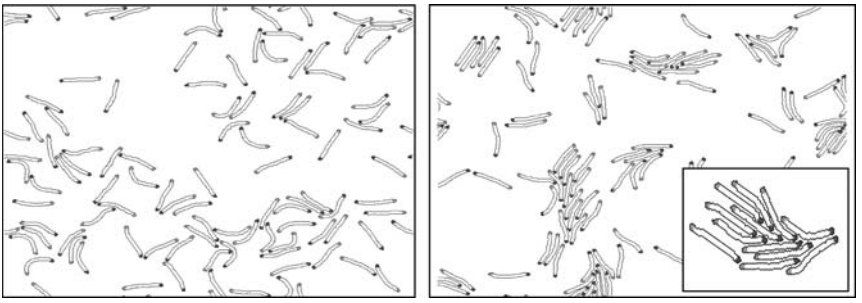

Fig. 6. Collective migration in simulated model cell populations. Starting from 100 randomly dropped cells a quasi steady state is reached, where cells mainly move collectively in clusters. A magnification of a particular arrow-like arrangement of cells within a cluster is shown in the inset image. Aspect ratio $\kappa \approx 10$. 'Heads' are marked with black dots.

3.2. Collective Migration

3.2.1. Cell Pattern of Collective Migration

Our main intention in this work is to answer the question whether a purely mechanical mechanism for collective migration is conceivable for *M. xanthus*. Collective migration is visible through the appearance of clusters of aligned cells, which move collectively in the same direction. Indeed, simulating a hundred cells, using the parameter set previously estimated for *M. xanthus*, already shows intense collective migration as predicted by our hypothesis (Fig. 6).

Aligned cell clusters arise in a characteristic arrow formation (Fig. 6, inset image) and allow collective migration of the cells. The whole cluster can change its moving direction upon a random turn of the leading cell(s). The arrow formation seems to enable cells in a cluster to follow cells in front of them.

3.2.2. Mechanism of Collective Migration

The central mechanism for collective migration is alignment upon cell collisions. Due to their active motion cells collide, interact via volume exclusion and end up with either parallel or anti-parallel orientation or do not align at all.[9]

Surprisingly we found out that the orientation after parallel alignment does not necessarily comply with the mean of both initial orientations. Figure 7 indicates how torque is produced during cell collisions due to persistent cell deformation, resulting in a cell orientation that is typically not the mean of the initial orientations.

[9] This latter can either be caused by too short interaction periods or by interactions that do not incorporate the leading cell segments of both cells. Especially cells with reduced stiffness would rather deform than align their heads.

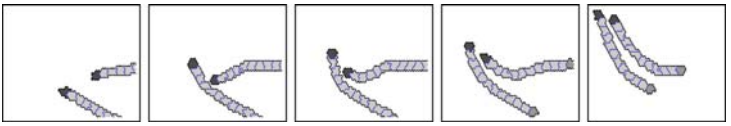

Fig. 7. Alignment of two colliding cells. The resulting orientation is not necessarily the mean of both initial orientations. The cell deformation upon collision can induce a torque resulting in a sustained change in cell orientation (parameter set 'xanthus').

Such a two-cell cluster keeps moving together for some characteristic time and meanwhile might incorporate a third cell or another cell cluster. By repetition of this process big clusters can evolve. The antagonistic process, cluster disintegration, is going on concurrently. Single cells break apart due to random changes in their moving direction and whole aligned clusters can subdivide into smaller clusters, e.g. upon collisions. If the cells arrange themselves in an arrow-like pattern, i.e. cells are not aligned exactly in parallel, but rather slightly turned into direction of the cluster's middle axis, a permanent force towards the middle axis of the arrow-like pattern results due to active motion of the individual cells. This force induces temporal stability of the cell cluster. The number of cells inside an aligned cell cluster as well as the aspect ratio of the cells obviously has an important impact on the characteristics of such a cell pattern.

3.2.3. Impact of Cell Properties on the Intensity of Collective Migration

As already mentioned, the 'microscopic' dynamics of collective migration are strongly affected by cell stiffness and aspect ratio. In order to quantify these effects on the 'macroscopic' patterns we introduce an order parameter for the intensity of collective migration – the average maximum cluster size $\bar{\Psi}$, that represents the competence of forming large aligned clusters. Central to this quantifier is the identification of clusters of cells, moving roughly into the same direction. Mathematically, we define two cells α, β to be next to each other within same cluster if they fulfil the following criteria:

$$D_{\max} > \min\{|\mathbf{S}_{\alpha,1} - \mathbf{S}_{\beta,1}|,\ |\mathbf{S}_{\alpha,1} - \mathbf{S}_{\beta,2}|, \ldots, |\mathbf{S}_{\alpha,1} - \mathbf{S}_{\beta,s}|, |\mathbf{S}_{\alpha,2} - \mathbf{S}_{\beta,1}|, \ldots, |\mathbf{S}_{\alpha,s} - \mathbf{S}_{\beta,s}|\} \tag{11}$$

$$\varphi_{\max} > \measuredangle(\theta_{\alpha,1}, \theta_{\beta,1}), \tag{12}$$

where $D_{\max}$ and $\varphi_{\max}$ are arbitrary constants, related to the maximum distance and maximum angle between the cells or moving directions, respectively ($D_{\max} = 8$ nodes, $\varphi_{\max} = \pi/4$). Using the criteria (11, 12) iteratively for all cell pairs α, β we can identify all cells belonging to the same cluster and calculate a cluster size distribution ψ at each time point of thejnodel simulation.

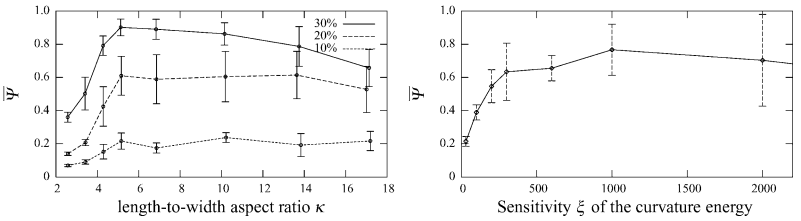

Fig. 8. The graphs show the impact of aspect ratio (*left*) and cell stiffness (*right*) on the intensity of collective migration. $\bar{\Psi}$ remains low until a critical aspect ratio of 4 and reaches a plateau for $\kappa = 5$. This result was obtained consistently for different cell densities (10, 20 or 30% of the nodes were occupied by cells). Also a minimum of cell stiffness is required to provide intense collective migration.

The average maximum cluster size $\bar{\Psi}$ was determined from ψ in the following way: initially a model cell population was allowed to establish a quasi steady state. Then the simulation was continued for a certain time during which the cluster size distribution ψ was determined at regular time intervals. Finally, $\bar{\Psi}$ was calculated as the average size of the largest cluster in all measured ψ, normalized by the population size. $\bar{\Psi} = 1$ indicates that the whole population moves collectively in a single cluster, whereas $\bar{\Psi} \to 0$ indicates 'no collective migration'.

Figure 8 shows how the single cell properties aspect ratio (through κ) and stiffness (through ξ,) relate to the population competence of collective migration. Both, low κ and low ξ, merely lead to no significant collective migration. Too short cells can not form aligned cell clusters with an 'arrow shape,' leading to increased disintegration of cell clusters. Also the probability of collisions and the persistence of motion is reduced (Fig. 5(b)). A minimal stiffness, however, ensures that the cells align rather than deform during their collision. This confirms that both a minimal stiffness and a minimal aspect ratio (two of our hypothetic assumptions) are essential for intense collective migration. If we compare our findings to the parameters we previously determined for *Myxococcus xanthus* ($\kappa \approx 6, \xi = 300\,\mathfrak{E}$) we can see almost optimal collective migration abilities for the cells.

The graphs also elucidate the counter-intuitive relation, that the intensity of collective migration saturates for $\kappa \geq 5$ and $\xi \geq 350\,\mathfrak{E}$. This effect appears for different cell densities. Both, increase of κ and ξ has a positive effect on the generation of aligned clusters, particularly by increasing the probability of collisions or alignments. Furthermore, the increase slows down the disintegration of clusters, especially by increasing the persistence into the moving direction. However, the resulting equilibrium of generation and disintegration does not reach the state where all cells are within one big aligned cluster, since due to stochastic cell motion cluster disintegration remains under all conditions. An additional disintegrating effect appears for large κ at high cell densities, where $\bar{\Psi}$ even decreases.

In that case cells deform during traffic jams and hence clusters disintegrate (see also Sec. 3.1).

The length-to-width aspect ratio κ is of particular importance for the collective migration, as it induces local cell alignments and stability of aligned clusters (see Sec. 3.2.2). This is reflected in the impact of κ on $\bar{\Psi}$, since there is a critical $\kappa_{cr} \approx 4$–5, below which the intensity of collective migration is low. A transition to intense collective migration can be seen at κ_{cr} for all cell densities analysed. This indicates, that the length-to-width aspect ratio essentially controls the collective migration.

4. CONCLUSIONS

In this paper we have introduced a *Cellular Potts Model* (CPM) representing rod-shaped cells that move actively along their long axis. This approach makes use of a 'set-of-lattice-nodes' cell representation in the CPM to define cells of specific shape and of certain stiffness, e.g. rod-shaped bacterial cells. We increased the spatial detail level of the original CPM by introducing the concept of a 'segmented cell' – a cell is now substructured into spatially separated segments. Optimal and suboptimal cell shapes are defined using energetic constraints for the spatial arrangement of the cell segments.

We have applied this concept to model rod-shaped cells of *M. xanthus* with a certain stiffness. We characterized the single cell behaviour by cell speed and orientation stability. The effect of cell stiffness is visible in the relaxation of an artificially bended model cell. Studying the complex behaviour of cell populations, we show our model to resemble the collective migration behaviour of gliding myxobacteria. Furthermore, we have studied the influence of the rod-like cell shape, cell stiffness and active motion on collective migration. In numerical simulations, using a parameter set estimated for *M. xanthus* and random initial conditions, we observed the emergence of aligned cell clusters and collective motion at the macroscopic level of cell populations. The formation of aligned cell clusters was found to be driven by local alignments due to collisions of the anisotropic cells. Stability of the aligned clusters in the presence of stochastic motion is provided by an arrow arrangement of the cells in the cluster, i.e. the moving direction of the cells within a cluster is slightly turned to the cluster's middle axis.

The intensity of collective migration in model cell populations, quantified through the average size of the largest aligned cluster, was analysed with respect to the impact of aspect ratio and stiffness of the cells. We observed a critical aspect ratio, above which intense collective migration occurs and saturates for even longer cells (Fig. 8). In an analogous way a minimal cell stiffness was found to be essential. The study of rigid rods is not possible with our model. However, a theoretical model was published covering exactly the collective behaviour of

self-propelled rigid rods. Peruani *et al.*[16] show that collective migration takes place also without the assumption of flexible rods. Whether the particles described in Ref. 16 can reach a comparable intensity of collective migration as our model is up to future analysis. The third of our hypothetic assumptions, active directed motion, was found to be essential too. Although anisotropic particles are able to form aligned clusters in the presence of Brownian motion, as indicated by the local alignment in liquid crystals, the stochastic motion in myxobacteria is some orders of magnitudes too low to allow alignment.

In summary we could show that collective migration takes place in populations of actively moving rod-shaped cells, provided they have a minimal stiffness and shape anisotropy. The local interaction in the underlying mechanism is mediated via volume exclusion and, contrary to known mechanisms of collective motion, no cooperation is involved. In addition, the results of Peruani *et al.*[16] indicate that the flexibility of the cells is not essential for the formation of collectively moving clusters.

In our model stability of cell clusters is provided by an arrow arrangement of the cells within a cluster, i.e. cells are aligned not exactly in parallel, but slightly turned towards the middle axis of the cluster. In *M. xanthus* additional cell interactions, particularly cell adhesion mediated through pili and fibrils, further contribute to cluster stability. Therefore, parallel cell arrangements in clusters, as observed in myxobacteria, are likely to be stable. In addition, considering cell adhesion would presumably increase cluster stability by decreasing the rate of cluster disintegration and thereby lead to even larger equilibrium cluster sizes. We point out the implication of the results on the self-organisation in the life cycle of *M. xanthus*, since clustering (local alignment) and collective migration turn out to be persistent properties of the cell population. In the streaming phase, when cells behave close to our model cells, aligned clusters of large size evolve and incorporate thousands of cells. In the spreading phase, when cells regularly reverse their moving direction, aligned cell clusters are much smaller. We suggest that the cluster formation mechanism we introduced might be perturbed by cell reversals, leading to lower cluster sizes.

Furthermore there is good agreement in the range of aspect-ratios found in vegetative cells of various myxobacteria strains (0.7 to 1.2 μm by 3 to 12 μm[5]) and those predicted to be optimal for collective migration by our model. Clearly we see a connection to evolutionary pressure on the ability of collective migration, since aligned cell clusters play an essential role in the early stages of fruiting body formation, an important step in the survival strategy of myxobacteria upon nutrient shortage.

Experimental validation of our predictions can be performed with *M. xanthus* cells. We suggest to use mutants that are unable to undergo cell reversal and which lack S-motility, i.e. they are unable to synthesize type IV pili. These cells have a

significantly reduced adhesivity and move persistently. We suggest to investigate the clustering intensity of such mutants inside of vegetative colonies. This allows to test the assumptions of our proposed mechanism for collective migration.

In the present study we have not included cell reversals. A rigorous study of the effect of cell reversal on collective migration remains for future research. Future problems will also concern the origin of more complex patterns, e.g. vortices and mounds. First indications on vortex formation have been observed in our model (data not shown). However, since vortex formation in myxobacteria has an intrinsic three-dimensional structure our model should be extended to a third dimension.

ACKNOWLEDGMENTS

We thank M. Bär (Berlin), T. Klauß (Dresden) and F. Peruani (Dresden) for fruitful discussions. This work was partially funded by DFG grant *DE 848/2-2*.

REFERENCES

1. M. Alber, M. Kiskowski and Y. Jiang, Lattice gas cellular automaton model for rippling and aggregation in myxobacteria. *Physica D* **191**:343–358 (2004).
2. U. Börner, A. Deutsch, H. Reichenbach and M. Bär, Rippling patterns in aggregates of myxobacteria arise from cell-cell collisions. *Phys. Rev. Lett.* **89**:078101 (2002).
3. J. H. Bussemarker, A. Deutsch and E. Geigant, Mean-field analysis of a dynamical phase transition in a cellular automaton model for collective motion. *Phys. Rev. Lett.* **78**:5018–5021 (1997).
4. A. Deutsch and S. Dormann, Cellular automaton modeling of biological pattern formation - characterization, applications, and analysis. Birkhauser, Boston (2005).
5. M. Dworkin and D. Kaiser, Myxobacteria II. American Society for Microbiology (1993).
6. F. Graner and J. A. Glazier, Simulation of biological cell sorting using a two-dimensional extended Potts model. *Phys. Rev. Lett.* **69**:2013–2016 (1992).
7. O. Igoshin, A. Mogilner, R. D. Welch, K. Dale and G. Oster, Pattern formation and traveling waves in myxobacteria: Theory and modeling. *Proc. Natl. Acad. Sci. U.S.A.* **98**:14913–14918 (2001).
8. O. A. Igoshin, R. Welch, D. Kaiser and G. Oster, Waves and aggregation patterns in myxobacteria. *Proc. Natl. Acad. Sci. U.S.A.* **101**:4256–4261 (2004).
9. L. Jelsbak and L. Søgaard-Andersen, Pattern formation by a cell surface-associated morphogen in *Myxococcus xanthus*. *Proc. Natl. Acad. Sci. U.S.A.* **99**:2032–2037 (2002).
10. D. Kaiser, Coupling cell movement to multicellular development in myxobacteria. *Nat. Rev. Microbiol.* **1**:45–54 (2003).
11. D. Kaiser and C. Crosby, Cell movement and its coordination in swarms of *Myxococcus xanthus*. *Cell. Motil. Cytoskeleton* **3**:227–245 (1983).
12. D. Kaiser and R. Yu, Reversing cell polarity: Evidence and hypothesis. *Curr. Opin. Microbiol.* **8**:216–221 (2005).
13. R. Merks, J. Glazier, S. Brodsky, M. Goligorksy and S. Newman, Cell elongation is key to in silico replication of in vitro vasculogenesis and subsequent remodeling. *Dev. Biol.* **289**:44–54 (2006).
14. A. Mogilner and L. Edelstein-Keshet, Spatio-angular order in populations of self-aligning objects: formation of oriented patches. *Physica D* **89**:346–367 (1996).

15. H. Othmer and P. Schaap, Oscillatory cAMP signaling in the development of *Dictyostelium discoideum*. *Comments Theor. Biol.* **5**:175–282 (1998).
16. F. Peruani, A. Deutsch and M. Br, Non-equilibrium clustering of self-propelled rods. *Phys. Rev. E* **74**:030904 (2006).
17. A. M. Rodriguez and A. M. Spormann, Genetic and molecular analysis of *cglb*, a gene essential for single-cell gliding in *Myxococcus xanthus*. *J. Bacteriol.* **181**:4381–390 (1999).
18. L. Søgaard-Andersen, Cell polarity, intercellular signalling and morphogenetic cell movements in *Myxococcus xanthus*. *Curr. Opin. Microbiol.* **7**:587–593 (2004).
19. W. Shi and D. R. Zusman, The two motility systems of *Myxococcus xanthus* show different selective advantages on various surfaces. *Proc. Natl. Acad. Sci. U.S.A.* **90**:3378–3382 (1993).
20. A. M. Spormann and D. Kaiser, Gliding movements in *Myxococcus xanthus*. *J. Bacteriol.* **177**:5846–5852 (1995).
21. A. Stevens, A stochastic cellular automaton modeling gliding and aggregation of myxobacteria. *SIAM J. Appl. Math.* **61**:172–182 (2000).
22. H. Sun, Z. Yang and W. Shi, Effect of cellular filamentation on adventurous and social gliding motility *of Myxococcus xanthus*. *Proc. Nat. Acad. Sci. U.S.A.* **96**:15178–15783 (1999).
23. T. Vicsek, A. Czirók, E. Ben-Jacob, I. Cohen and O. Shochet, Novel type of phase transition in a system of self-driven particles. *Phys. Rev. Lett.* **75**:1226–1229 (1995).
24. R. Welch and D. Kaiser, Cell behavior in traveling wave patterns of myxobacteria. *Proc. Natl. Acad. Sci. U.S.A.* **98**:14907–14912 (2001).